Formation onset of flat-perylene prenucleation clusters in vacuum

Formation Onset of Flat-Perylene Prenucleation Clusters in Vacuum

Dilfuza Husanova[a], Jurat Ochilov[a], Umedjon Khalilov[b,c,d],

[a] Arifov Institute of Ion-Plasma and Laser Technologies, Academy of Sciences of Uzbekistan, Tashkent 100125, Uzbekistan

[b] New Uzbekistan University, Tashkent 100007, Uzbekistan

[c] Central Asian University, Tashkent 111221, Uzbekistan

[d] University of Antwerp, Antwerp 2610, Belgium

e-mail: umedjon.khalilov@uantwerpen.be

Our current understanding of the prenucleation processes involved in the growth of perylene-based organic nanocrystals is still limited. In this study, we utilized molecular dynamics simulations, employing various flat perylene molecules, to investigate these processes. Our findings reveal that, while cluster formation is primarily driven by molecular aggregation, the Ostwald ripening phenomenon also occurs in a vacuum environment. The presence of a methoxy group influences both the rate and structure of clustering. Interestingly, the preferred initial clusters, as determined by their molar Gibbs free energies, do not align with the crystal units or nuclei observed in herringbone perylene crystals. Overall, this study enhances the understanding of organic nanocrystal formation, specifically nonclassical nucleation pathways, and guides the manipulation of perylene-based organic crystals.

Keywords: Organic nanocrystals, Flat perylene molecules, Prenucleation mechanism, Molecular dynamics

Introduction

The high reputation of organic materials in tailor-made molecular structures and low-cost manufacturing processes make them more advantageous than their inorganic counterparts in research areas of next-generation carbon nanotechnology, including organic photocatalysis, organic optoelectronics, organic superconductors, organic photonics, and organic spintronics. [1–11]. Among them, much attention is given to organic optoelectronic materials due to theirapplication in nanodevices, such as organic light-emitting diodes [5], organic photoconductors [8], and organic solar cells [4]. In the design of organic optoelectronic materials, polycyclic aromatic hydrocarbons (PAHs), a rigid conjugate system, play a prominent role [1,12]. In particular, perylene and its derivatives are ideal candidates among well-known PAHs due to their very appealing electronic properties [1,12]. Namely, this group of materials has a broad intermolecular interaction potential dominated by nonbonding interactions [12,13].

In general, various fabrication techniques, such as the reprecipitation method [14], supercritical fluid crystallization method [15], microwave-irradiation reprecipitation method [16], and mass production of organic nanocrystals [17], are used for the synthesis of ONCs. Reprecipitation is a convenient synthesis method for the synthesis of ONCs with controlled size and morphology, including for perylene-based ONCs [6]. Several ONCs, such as nonlinear optical dyes, fullerene, polymers, and fluorescent dyes [1,6,10], are widely fabricated using this method. In this method, organic molecules are rapidly exposed to a weak solvent environment, which induces nucleation and subsequent growth into ONCs. Subsequently, several parameters, including temperature and stirring rate, can be tuned to control the morphology and size of ONCs [1,6].

Recent studies strongly indicate that a deeper understanding of the nucleation mechanisms is essential for the successful selective synthesis of ONCs [3,18]. Consequently, two main theories are used to explain the mechanisms of the initial stage of ONC growth: classical nucleation theory (CNT) [3,18,19] and nonclassical nucleation theory (NCNT) [20,21]. Both theories have successfully explained experimental results to some extent; however, there are still two different views on the explanation of the crystal nucleation process [22]. In general, CNT proposes that critical nuclei serve as transitions between supersaturated solutions and growing particles. The additional energy of these nuclei relies on supersaturation and affects the barrier height for phase separation [3]. However, the theory assumes idealized conditions and neglects many factors that may influence nucleation, such as surface effects, nonequilibrium dynamics, or specific interactions within the system [23,24]. Therefore, CNTs may not fully capture the complexity of organic nanocrystal growth [23,25]. On the other hand, NCNT takes into account these additional factors [9]. Consequently, the theory explains the crystal nucleation process as consisting of two main stages, i.e., (i) the appearance of clusters during prenucleation processes and then (ii) a crystal-ordered nucleus within these clusters [22,26,27].

Understanding prenucleation processes is crucial for controlling and manipulating the growth of nanocrystals with desired properties [20,22]. NCNT provides a framework for exploring prenucleation processes [26] and offers insights into the complex phenomena occurring at the early stages of nucleation [21,24]. While experimental techniques [27-29] and molecular simulations [30,31] are being validated, the predictions of NCNT for a better understanding of prenucleation processes, formation mechanisms, and structure/morphology of prenucleation clusters in these processes are still not fully understood [3,22,24,32].

In this research, we aim to understand the mechanisms of prenucleation processes of ONCs consisting of aromatic hydrocarbon molecules in a vacuum environment (where there is an absence of surrounding molecules or a gaseous medium), applying computer simulations considering the available experimental evidence and theoretical hypotheses. In particular, we study the nature of the prenucleation process of ONC growth from selected flat perylene molecules in a vacuum at room temperature using molecular dynamics (MD) simulations.

Computational details

Perylene, a polycyclic aromatic hydrocarbon, is formed by combining two naphthalene molecules ($C_{10}H_6$). The molecule consists of three functional groups: *peri*, bay, and ortho, with twelve functional positions in total (see Fig. 1a). The *peri* group includes positions III, IV, IX, and X, the bay group includes positions I, VI, VII, and XII, and the ortho group includes positions II, V, VIII, and XI [7]. In addition to the original perylene molecule ($C_{20}H_{12}$) shown in Fig. 1 b, two derivatives are depicted in Fig. 1c and d. The first derivative, 1-methoxyperylene ($C_{21}H_{14}O$) (see Fig. 1c), is obtained by attaching a methoxy group to position VI of the perylene molecule. The second derivative, 4,10-dimethoxy-1,2,3,6b,7,8,9,12b-octahydroperylene ($C_{22}H_{24}O_2$) (see Fig. 1d), is formed by attaching methoxy groups to positions III and IX. These perylene molecules function as building blocks in the crystals PERLEN08 [33], WUFJEM [34], and RELVUC [35], as identified by the reference codes in the Cambridge Structural Database (CSD). For simplicity, we use the names PERLEN08, WUFJEM, and RELVUC to represent the molecules $C_{20}H_{12}$, $C_{21}H_{14}O$, and $C_{22}H_{24}O_2$, respectively.

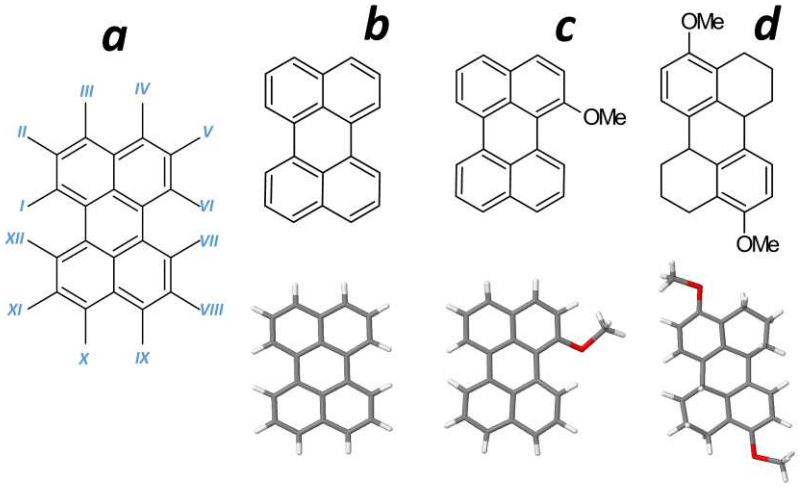

Fig. 1 (a) Twelve functional positions of the flat perylene molecule. The structures of (b) PERYLENE08 ($C_{20}H_{12}$), (c) WUFJEM ($C_{21}H_{14}O$) and (d) RELVUC ($C_{22}H_{24}O_2$) molecules. In molecules (in the bottom), C, H and O atoms are represented in gray, white and red colors, respectively. (For interpretation of the references to colour in this figure legend, the reader is referred to the web version of this article.)

To investigate the formation of prenucleation clusters, these three perylene molecules are selected for MD simulations. The interactions between atoms in the system are described by the ReaxFF potential [36,37] using a parameter set introduced by Zhang and colleagues [38]. The simulations are conducted using the LAMMPS software package [39], which is based on the MD algorithm.

The simulation of perylene molecule clustering is conducted using the NVT ensemble, where N denotes the number of atoms in the system, V represents the volume of the simulation box, and T signifies the constant temperature of the system. By maintaining these parameters constant, the NVT ensemble accurately represents the clustering dynamics and allows for the study of associated properties. The simulation box contains 64 perylene molecules, consisting of 2048 atoms for PERLEN08, 2304 atoms for WUFJEM, and 3072 atoms for RELVUC. The box sizes for the three molecule cases are chosen as 72.58 × 59.53 × 57.74 Å3, 72.68 × 62.83 × 69.66 Å3, and 83.82 × 58.36 × 63.38 Å3, respectively. Hence, molecules are uniformly distributed in the simulation box with periodic boundary conditions. This eliminates edge effects and accurately represents the clustering process by creating an infinite system. The periodic boundary conditions allow molecules to freely move and interact with their periodic images, improving the reliability of

the simulation results. A Nose-Hoover thermostat with a coupling constant of 100 fs [40] is employed to maintain a constant temperature of approximately 300 K. This thermostat periodically adjusts the particle velocities based on temperature, ensuring temperature stability throughout the simulation. The careful selection of a coupling constant of 100 fs plays a crucial role in regulating the temperature during the simulation, ensuring efficient and accurate control over the system's thermal behavior.

A time step of 0.5 fs is used for the MD integration scheme in the simulations, governing the update frequency of particle positions and velocities. The total duration of the simulations is set to 2.5 ns, which determines the length of time over which the system dynamics are studied. The trajectory of the system atoms is recorded and saved at regular intervals of 1 ps during the simulation. Simulations are repeated five times for each case, and the parameters obtained are averaged, ensuring a robust and representative analysis while minimizing the impact of random fluctuations.

Results and discussion

Fig. 2 shows, as an example, the evolution of the formation of a perylene cluster consisting of 64 WUFJEM molecules. During the prenucleation process, the number of clusters with varying sizes, each containing a different number of molecules, increases. In a vacuum, perylene clusters can emerge through a combination of intermolecular interactions, including π-π stacking, van der Waals forces, and electrostatic interactions [13]. These molecular interactions facilitate the formation of perylene clusters starting from dimers, which then extend to trimers, tetramers, and small molecular compounds (clusters) and ultimately develop into complete clusters [31].

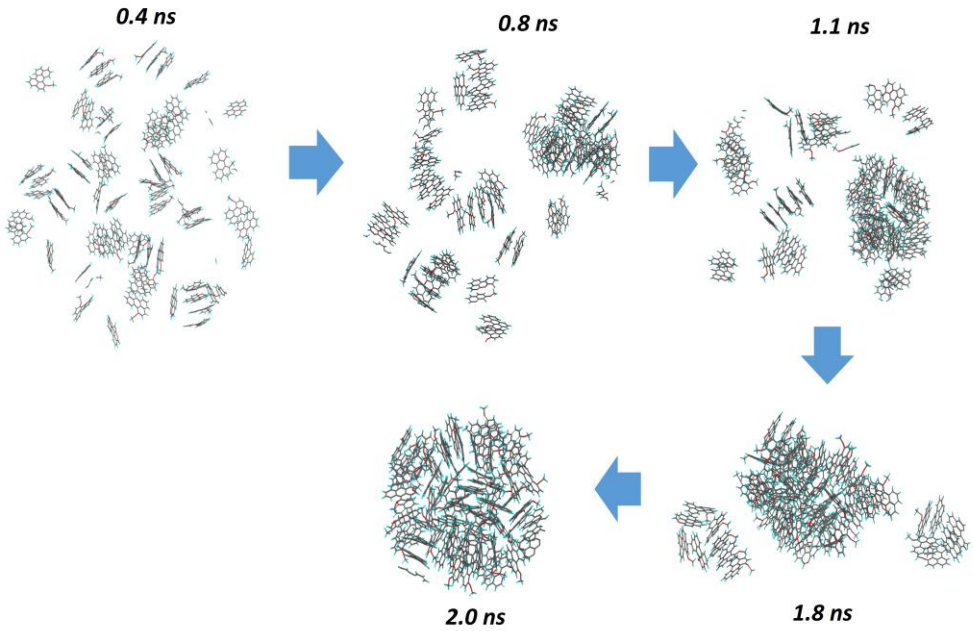

Fig. 2 Evolution of WUFJEM cluster formation

Generally, perylene clusters in a certain solution, e.g., in a water environment, are formed through the self-assembly of perylene molecules driven by hydrophobic interactions, π-π stacking, and van der Waals forces [13]. The hydrophobic nature of these molecules compels them to minimize contact with water, resulting in aggregation [41,42]. When perylene molecules are placed in a vacuum, they gain freedom of movement and interaction without the constraints imposed by surrounding solution molecules [21]. Simulation results demonstrate that Ostwald ripening [43 –45] can occur concurrently with molecular assembly or cluster formation in a vacuum environment. According to the Ostwald

ripening rule, larger clusters continue to grow, while smaller clusters shrink until they revert to monomers [45]. In our study, as a trimer transforms into a dimer and then into a monomer, the remaining monomers adhere to larger clusters, which exhibit a significantly lower chemical potential than that of the monomer. This phenomenon predominantly occurs when face-to-edge (*T*-shaped) dimers or trimers, based on these dimers, are formed. The explanation lies in the interaction energy among these molecules, which is weaker than the average kinetic energy of these molecules ($5/2 \cdot k_B T$, where k_B is the Boltzmann constant, and T is the room temperature), approximately 0.065 eV [46]. Additionally, our calculations indicate that initial molecular assemblies in the case of PERLEN08 are less stable than those in the cases of WUFJEM and RELVUC. However, in most cases, the mutual interaction energy is much higher than the average kinetic energy. Therefore, the occurrence of the Ostwald ripening phenomenon is rare compared to the occurrence of molecular aggregation during the cluster formation process. Consequently, over time, the latter phenomenon leads to the growth of larger clusters at the expense of smaller ones. The larger clusters become more stable and dominant as they gain molecules from the smaller clusters. The overall findings reveal that the clustering behavior of PERLEN08 and RELVUC molecules closely resembles that of the WUFJEM case. However, there are distinct differences in their clustering rates, indicating variations in the kinetics of cluster formation.

The kinetics of aggregation or clustering among molecules are strongly influenced by the nature of their interactions. As illustrated in Fig. 3, the formation time of molecular dimers, trimers, tetramers, semi-clusters (defined as a cluster containing half of the total system molecules) and complete clusters (defined as a cluster containing all system molecules) varies depending on the type of molecule. In particular, the formation of molecular dimers takes 0.32 ns, 0.38 ns, and 0.30 ns for PERLEN08, WUFJEM, and RELVUC molecules, respectively. Subsequently, the formation times for trimers and tetramers are 0.39 ns and 0.40 ns for PERLEN08, 0.46 ns and 0.55 ns for WUFJEM, and 0.42 ns and 0.42 ns for RELVUC. Interestingly, although the rate of preassembly formation is relatively high for PERLEN08 molecules compared to the others, the formation times of the semi-cluster and complete PERLEN08 cluster become lower compared to the other cases. Specifically, the formation of the PERLEN08 semi-cluster experiences delays of 0.02 ns and 0.14 ns compared to the WUFJEM and RELVUC semi-clusters, respectively. The delays become significant for the formation of the complete cluster, amounting to 6.05 ns and 6.93 ns, respectively. The presence of methoxy groups in perylene molecules plays a crucial role in promoting the clustering process by facilitating hydrogen bond formation between neighboring molecules.

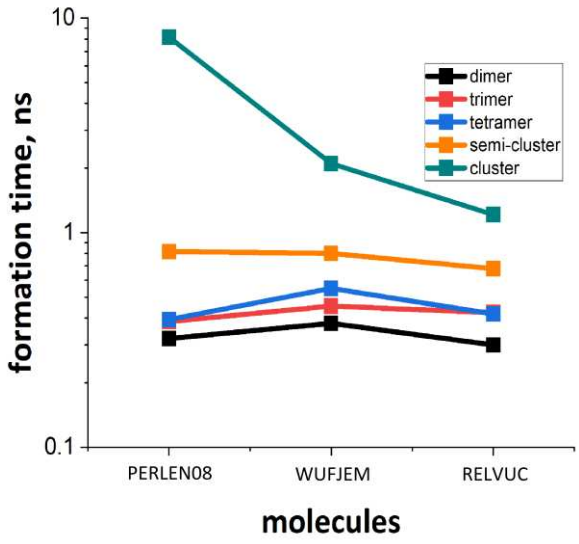

Fig. 3 Cluster formation rate of flat perylene molecules.

This enhanced interaction, primarily driven by hydrogen bonding, leads to the accelerated formation of semi- and complete clusters, particularly observed in the cases of WUVJEM and RELVUC. The overall results highlight the notable influence of oxygen atoms on the dynamics of perylene clustering.

The overall results show that perylene molecules mainly assemble in two orientations, i.e., face-to-face (or parallel) and face-to-edge (or *T*-shaped), during the clustering process. To develop a thorough understanding of the onset of clustering, the analysis specifically examines the formation of initial structures, represented by dimers, trimers, and tetramers, as depicted in Fig. 4. This analysis involves assessing both the interaction energy between newly introduced molecules and existing clusters or individual molecules, as well as evaluating the stability of the resulting clusters. A detailed examination of these factors allows for valuable insights into the initiation of clustering and the stability of the resulting structures. In particular, the energy of interaction of a molecule with another molecule or a cluster is expressed as $E = E_{mol-clus} - (E_{mol} + E_{clus})$ [47], where $E_{mol\text{-}clus}$ is the potential energy of a newly formed cluster (or molecular assembly), E_{mol} is the potential energy of the perylene molecule, and E_{clus} is the potential energy of the cluster (or the molecular assembly). Additionally, the relative stability of the aggregation of the molecules is evaluated by the molar Gibbs free energy (ΔG_m), which is calculated as $\Delta G_m = E_{coh} - \sum \chi_i \mu_i$ [48–51], where E_{coh} is the cohesive energy of the cluster and χ_i and μ_i are the relative concentration of the type i atom (C or H or O) and its chemical potential, respectively. In our case, the relative concentrations of atoms in the appropriate state are $\chi_C = 0.625$, $\chi_H = 0.375$ and $\chi_O = 0.0$ for PERLEN08, $\chi_C = 0.5833$, $\chi_H = 0.3889$ and $\chi_O = 0.0278$ for WUFJEM and $\chi_C = 0.4583$, $\chi_H = 0.5$ and $\chi_O = 0.0417$ for RELVUC. The chemical potentials of C, H and O atoms correspond to the cohesive energy of infinite graphite (μ_C = -7.64 eV/atom), the binding energy per atom of the H_2 (μ_H = -2.36 eV/atom) and O_2 molecule (μ_O = -2.30 eV/atom), respectively.

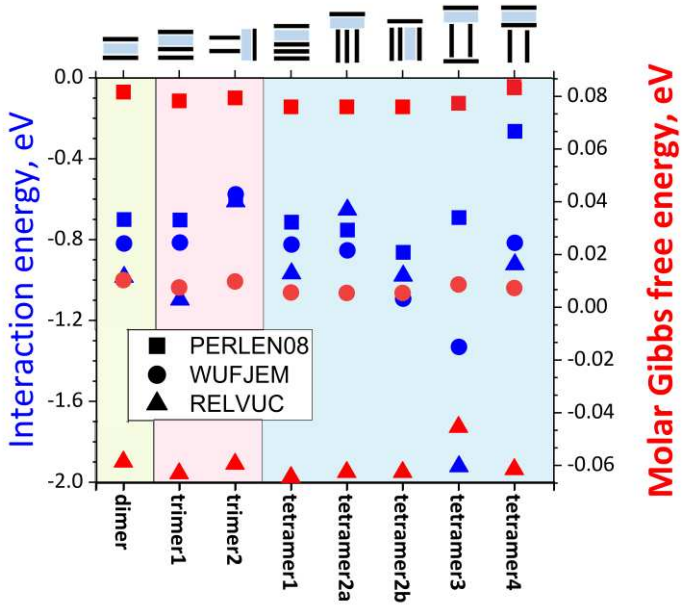

Fig. 4 Interaction energy of a monomer (molecule) with a cluster, as well as the molar Gibbs free energy of the resulting perylene cluster.

During the initial stages of the prenucleation process, the first dominant configuration is a dimer, where molecules align mainly parallel to each other or in a face-to-face orientation (as shown in Fig. 3, dimer). This arrangement is facilitated by the formation of π-π bonds between carbon atoms in neighboring perylene molecules [47,51]. Namely, the aromatic rings in perylene molecules can engage in π-π stacking interactions, which entail the alignment and overlapping of their π-electron clouds [13,47,51]. According to the calculations, the partial charges on the hydrogen and carbon atoms in

flat perylene molecules are 0.042e and −0.032e for PERLEN08, 0.052e and −0.011e for WUFJEM, and 0.053e and −0.014e for RELVUC, respectively. As a result, the electrostatic interactions as well as the London dispersion nature lead to the formation of noncovalent C---H bonds between neighboring molecules [36]. Consequently, flat perylene molecules tend to accumulate in a face-to-edge (*T*-shaped) orientation [35,51]. However, the stability of *T*-shaped dimers in all perylene molecules is notably lower compared to the observed stability in parallel dimers. This difference highlights the unique energy landscape and structural limitations involved in the formation of *T*-shaped dimers, indicating their lower stability compared to parallel dimers. Furthermore, the presence of an oxygen atom in the WUFJEM and RELVUC molecules leads to partial charges of approximately −0.50446 e and −0.48419 e, respectively, on the oxygen atom. As a result, in the case of WUFJEM and RELVUC molecules, the formation of hydrogen bonds (H---O) between the hydrogen and oxygen atoms of neighboring molecules aids in their assembly, particularly facilitating their face-to-face arrangement [38]. Due to the aforementioned intermolecular interactions, the energy of interaction between flat perylene molecules exhibits distinct values. Specifically, the PERLEN08, WUFJEM, and RELVUC molecules demonstrate interaction energies of −0.701 eV, −0.820 eV, and −0.985 eV, respectively. The face-to-face configuration of the PERLEN08 dimer demonstrates a more favorable interaction energy (-0.70 eV) compared to the face-to-edge configuration (-0.27 eV), despite the absence of the latter in Fig. 4. These energy values closely correspond to previously reported experimental, computational, or theoretical results, which indicate values of −0.30 to −0.70 eV for parallel dimers [47,51,52] and −0.21 eV for *T*-shaped dimers [51]. In face-to-face dimers, there is a consistent increase in the energy required for dimer formation as the number of oxygen atoms in the molecules increases. This observation suggests a direct relationship between the interaction energy and the formation of hydrogen bonds between molecules. Hydrogen bond formation plays a critical role in determining the relative stability of the dimers. Specifically, these hydrogen bonds contribute to the increased stability of the RELVUC dimer compared to the WUFJEM dimer, as well as the enhanced stability of the WUFJEM dimer compared to the PERLEN08 dimer. The stability trend is evident in the molar Gibbs energies, with the RELVUC dimer (ΔG_m = -0.059 eV) demonstrating the highest stability, followed by the WUFJEM dimer (ΔG_m = 0.010 eV), while the PERLEN08 dimer (ΔG_m = 0.082 eV) exhibits the lowest stability.

Subsequently, the next molecule in the sequence joins the dimer either in a face-to-face orientation (referred to as trimer1 in Fig. 4) or in a face-to-edge orientation (referred to as trimer2 in Fig. 4), driven by the abovementioned noncovalent interactions. The results indicate that the interaction energy of the third molecule in the face-to-face orientation is higher than the interaction energy of the third molecule in the face-to-edge orientation for all three molecules. Specifically, the interaction energy values are −0.703 eV, −0.815 eV, and −1.098 eV for PERLEN08, WUFJEM, and RELVUC, respectively, in the face-to-face orientation, while the values are −0.594 eV, −0.576 eV, and −0.612 eV for PERLEN08, WUFJEM, and RELVUC, respectively, in the face-to-edge orientation. According to the molar Gibbs energy calculations, it is also observed that the trimer1 clusters of all perylene molecules are more stable than their trimer2 clusters. Specifically, the molar Gibbs energy values for the trimer1 clusters are determined to be 0.078 eV, 0.008 eV, and −0.063 eV for PERLEN08, WUFJEM, and RELVUC, respectively. Similarly, the molar Gibbs energy values for the trimer2 clusters are found to be 0.080 eV, 0.010 eV, and −0.060 eV for PERLEN08, WUFJEM, and RELVUC, respectively. Overall, the face-to-face orientation shows a higher interaction energy between the third molecule and the dimer, resulting in greater stability of trimer1 clusters compared to trimer2 clusters, as indicated by molar Gibbs energy calculations.

When the next molecule is incorporated into either trimer1 or trimer2, it can result in the formation of four distinct configurations of tetramers, represented as tetramer1-4 in Fig. 4. In particular, the interaction energies between the fourth perylene molecule and the cluster range from −0.653 eV to −1.092 eV for the tetramer1 and tetramer2 states, while for tetramer3 and tetramer4, the range expands from −0.264 eV to −1.922 eV. While the interaction energies with the incoming molecule may be different, the overall stability of the resulting cluster plays a crucial role in determining subsequent structure formation. Specifically, the WUFJEM or RELVUC molecule shows a strong

preference for joining the trimer2 cluster in a face-to-edge orientation, resulting in tetramer3 clusters with interaction energies of −1.331 eV for WUFJEM and −1.922 eV for RELVUC. Nevertheless, the molar Gibbs free energies (ranging from 0.076 to 0.083 eV for PERLEN08, 0.005 to 0.009 eV for WUFJEM, and −0.064 to −0.045 eV for RELVUC) indicate that the tetramer3 clusters exhibit the lowest stability compared to the other tetramer clusters. The results indicate an average stability difference of approximately 0.07 eV between PERLEN08 and WUFJEM tetramers, as well as between WUFJEM and RELVUC tetramers. This disparity in perylene stability can be attributed to variations in the number of oxygen atoms or hydrogen bonds present in the clusters. Additionally, it is observed that the average stability of the clusters consistently increases by approximately 6 meV with the addition of each successive molecule to the cluster in all three perylene cases.

The analysis of the overall stability scheme reveals interesting patterns in the aggregation of the three perylene molecules. The transition from dimer to trimer1 clusters leads to the formation of either tetramer1 or tetramer2 structures. In the case of PERLEN08, both tetramer1 and tetramer2 configurations demonstrate favorable stability (G_m = 0.076 eV), suggesting that PERLEN08 molecules can adopt either structure with comparable stability. However, WUFJEM molecules exhibit a notable preference for the tetramer2 structure, which emerges as the more stable configuration. Molar Gibbs free energies indicate a stronger inclination for WUFJEM molecules to form tetramer2 (G_m = 0.005 eV), indicating that it is the preferred arrangement for achieving enhanced stability. In contrast, the RELVUC case exhibits a clear preference for the tetramer1 structure, which displays the highest stability (G_m = -0.064 eV) among the considered configurations. RELVUC molecules strongly tend to form tetramer1 clusters, suggesting that this arrangement maximizes their stability.

In all cases, it is worth highlighting that the tetramer1 and tetramer2 clusters, despite their favorable stability, do not align with the crystal units or nuclei of α or β perylene crystals (as considered in tetramer4 in Fig. 4) [53,54]. This observation indicates that the formation of perylene-based organic crystals follows nonclassical nucleation pathways, offering new insights into the prenucleation process [3,22,27,55].

Conclusion

In this simulation-based research, our focus is on exploring the initial stages of organic nanocrystal formation, specifically the prenucleation processes. In particular, we employ molecular dynamics simulations to study the formation onset of nanocrystals from flat-perylene molecules. The results demonstrate that the clustering of perylene molecules occurs in a vacuum, relying on intermolecular interactions such as π-π stacking and van der Waals forces (including hydrogen bonding), without the presence of a solvent or external factors. Additionally, we observed that larger particles grow at the expense of smaller particles, a phenomenon known as Ostwald ripening. Specifically, 'incipient' clusters are reduced to monomers, and the monomers then reattach to larger clusters, resulting in the dominance of more stable particles during the cluster formation stage. Notably, the oxygen atoms within perylene molecules play a crucial role in promoting clustering by facilitating hydrogen bond formation. This enhanced interaction, driven by hydrogen bonding, speeds up the formation of partially formed and fully formed clusters. Interestingly, the preferred clusters, called tetramer1 and tetramer2, where the fourth molecule connects either face-to-face or face-to-edge with a parallel stacked trimer cluster, do not align with the crystal units or nuclei of α or β perylene crystals. This finding improves our understanding of the mechanisms involved in the early stages of crystal formation in an only vacuum environment and highlights the importance of nontraditional pathways in explaining how perylene-based organic crystals begin to form.

Acknowledgment

This research work was carried out within the framework of the fundamental project F-FA-2021-512 funded by the Agency for Innovative Development of the Republic of Uzbekistan. Simulations were carried out using the supercomputer cluster of the Institute of Ion-Plasma and Laser Technologies of the Academy of Sciences of Uzbekistan.

References

[1] O. Ostroverkhova, Organic optoelectronic materials: mechanisms and applications, Chem. Rev. 116 (22) (2016) 13279–13412.
[2] R. Li, et al., Micro-and nanocrystals of organic semiconductors, Acc. Chem. Res. 43 (4) (2010) 529– 540.
[3] R.J. Davey, S.L.M. Schroeder, J.H. Ter Horst, "Nucleation of organic crystals - a molecular perspective, Angewandte Chemie International Edition 52(8) (2013) 2166–2179.
[4] K.Y. Law, Organic photoconductive materials: recent trends and developments, Chem. Rev. 93 (1) (1993) 449–486.
[5] Q. Li, Z. Li, Molecular packing: another key point for the performance of organic and polymeric optoelectronic materials, Acc. Chem. Res. 53 (4) (2020) 962–973.
[6] K. Baba, et al. "Functional organic nanocrystals." Nanocrystals, ed. Y. Masuda (IntechOpen, 2011) Ch 15 (2011): 397.
[7] C. Li, H. Wonneberger, Perylene imides for organic photovoltaics: yesterday, today, and tomorrow, Adv. Mater. 24 (5) (2012) 613–636.
[8] Y. Sato, S. Ichinosawa, H. Kanai, Operation characteristics and degradation of organic electroluminescent devices, IEEE J. Sel. Top. Quantum Electron. 4 (1) (1998) 40–48.
[9] H. Zollinger, Color chemistry: syntheses, properties, and applications of organic dyes and pigments, John Wiley & Sons, 2003.
[10] T. Ishizaka, et al., Unique luminescence p roperties of Eu^{3+}-doped polyimide, J. Photochem. Photobiol. A Chem. 183 (3) (2006) 280–284.
[11] C. Huang, S. Barlow, S.R. Marder, Perylene-3, 4, 9, 10-tetracarboxylic acid diimides: synthesis, physical properties, and use in organic electronics, J. Org. Chem. 76 (8) (2011) 2386–2407.
[12] C. Sutton, C.a. Risko, J.-L. Bredas, Noncovalent intermolecular interactions in organic electronic materials: implications for the molecular packing vs electronic properties of acenes, Chem. Mater. 28 (1) (2016) 3–16.
[13] Z.-F. Yao, J.-Y. Wang, J. Pei, Control of π–π stacking via crystal engineering in organic conjugated small molecule crystals, Cryst. Growth Des. 18 (1) (2018) 7–15.
[14] H. Kasai, et al., A novel preparation method of organic microcrystals, Jpn. J. Appl. Phys. 31 (1992) L1132.
[15] Y. Komai et al., Size and form control of titanylphthalocyanine microcrystals by supercritical fluid crystallization method, Mol. Cryst. Liq. Cryst. Sci. Technol. Sect. Mol. Cryst. Liq. Cryst. 322 (1) (1998) 167–172.
[16] K. Baba, H. Kasai, S. Okada, H. Oikawa, H. Nakanishi, Novel fabrication process of organic microcrystals using microwave-irradiation, Jpn. J. Appl. Phys. 39 (2000) L1256.
[17] K. Ujiiye-Ishii, et al., Mass-production of pigment nanocrystals by the reprecipitation method and their encapsulation, Mol. Cryst. Liq. Cryst. 445 (1) (2006) 177–467.
[18] D. Erdemir, A.Y. Lee, A.S. Myerson, Nucleation of crystals from solution: classical and two-step models, Acc. Chem. Res. 42 (5) (2009) 621–629.
[19] D. Gebauer, et al., On classical and non-classical views on nucleation, Am. J. Sci. 318 (9) (2018) 969–988.
[20] P.G. Vekilov, Two-step mechanism for the nucleation of crystals from solution, J. Cryst. Growth. 275 (1–2) (2005) 65–76.
[21] P.G. Vekilov, Nucleation, Cryst. Growth Des. 10 (12) (2010) 5007–5019.
[22] D. Gebauer, et al., Pre-nucleation clusters as solute precursors in crystallisation, Chem. Soc. Rev. 43 (7) (2014) 2348–2371.
[23] D. Gebauer, S.E. Wolf, Designing solid materials from their solute state: a shift in paradigms toward a holistic approach in functional materials chemistry, J. Am. Chem. Soc. 141 (11) (2019) 4490–4504.
[24] S. Jeon, et al., Reversible disorder-order transitions in atomic crystal nucleation, Science 371 (6528) (2021) 498–503.
[25] P.R. Wolde ten, and Daan Frenkel. Enhancement of protein crystal nucleation by critical density fluctuations, Science 277 (1997) 1975-1978
[26] W.J. Habraken, et al., "Ion-association complexes unite classical and non-classical theories for the biomimetic nucleation of calcium phosphate, Nat. Commun. 4 (1) (2013) 1507.
[27] Y. Tsarfati, et al., "Crystallization of organic molecules: nonclassical mechanism revealed by direct imaging", ACS Central Sci. 4 (8) (2018) 1031–1036.

[28] D. Gebauer, A. Volkel, H. Colfen, Stable prenucleation calcium carbonate clusters, Science 322 (5909) (2008) 1819–1822.

[29] M. Beigmohamadi, et al., Structure and morphology of perylene films grown on different substrates, J. Appl. Phys. 104 (1) (2008) 013505.

[30] G.C. Sosso, et al., Crystal nucleation in liquids: Open questions and future challenges in molecular dynamics simulations, Chem. Rev. 116 (12) (2016) 7078–7116.

[31] U. Khalilov, et al., "Growth onset of perylene-based nanocrystals", Uzbek J. Phys. 23 (3) (2021) 7–11.

[32] T. Nakamuro, et al., Capturing the moment of emergence of crystal nucleus from disorder, J. Am. Chem. Soc. 143 (4) (2021) 1763–1767.

[33] J. Merz, et al., Synthesis, photophysical and electronic properties of tetra-donor-or acceptor- substituted ortho-perylenes displaying four reversible oxidations or reductions, Chem. Sci. 10 (32) (2019) 7516–7534.

[34] Š. Vyskočil, et al., 2, 8′-Disubstituted-1, 1′-Binaphthyls: A New Pattern in Chiral Ligands, Chem. A Eur. J. 8 (20) (2002) 4633–4648.

[35] J.F. Fuini, et al., The photophysical characterisation of novel 3, 9-dialkyloxy-and diacyloxyperylenes, Dyes Pigm. 88 (2) (2011) 204–211.

[36] A.C.T. Van Duin, C.T. Adri, et al., ReaxFF: a reactive force field for hydrocarbons, Chem. A Eur. J. 105 (41) (2001) 9396–9409.

[37] Q. Mao, A.C.T. Van Duin, K.H. Luo, Formation of incipient soot particles from polycyclic aromatic hydrocarbons: a ReaxFF molecular dynamics study, Carbon 121 (2017) 380–388.

[38] W. Zhang, A.C.T. Van Duin, Improvement of the ReaxFF description for functionalized hydrocarbon/water weak interactions in the condensed phase, J. Phys. Chem. B 122 (14) (2018) 4083–4092.

[39] A.P. Thompson, et al., LAMMPS-a flexible simulation tool for particle-based materials modeling at the atomic, meso, and continuum scales, Comput. Phys. Commun. 271 (2022) 108171.

[40] S. Nosé, A molecular dynamics method for simulations in the canonical ensemble, Mol. Phys. 52 (2) (1984) 255–268.

[41] M.R. Hestenes, E. Stiefel, Methods of conjugate gradients for solving linear systems, J. Res. National Bureau of Standard. 49 (1952) 409–438.

[42] J.J. Yoreo J. James, P.G. Vekilov, Principles of crystal nucleation and growth, Rev. Mineral. Geochem. 54 (1) (2003) 57–93.

[43] N.T.K. Thanh, N. Maclean, S. Mahiddine, Mechanisms of nucleation and growth of nanoparticles in solution, Chem. Rev. 114 (15) (2014) 7610–7630.

[44] U. Khalilov, et al., Nanoscale mechanisms of CNT growth and etching in plasma environment, J. Phys. D: Appl. Phys. 50 (18) (2017) 184001.

[45] A.M. Streets, S.R. Quake, Ostwald ripening of clusters during protein crystallization, Phys. Rev. Lett. 104 (17) (2010) 178102.

[46] U. Khalilov, et al., Can endohedral transition metals enhance hydrogen storage in carbon nanotubes?, Int. J. Hydrogen Energy. 55 (15) (2024) 604–610.

[47] I.A. Fedorov, Y.N. Zhuravlev, V.P. Berveno, Structural and electronic properties of perylene from first principles calculations, J. Chem. Phys. 138 (9) (2013) 03B605.

[48] T. Dumitrică, M. Hua, B.I. Yakobson, Endohedral silicon nanotubes as thinnest silicide wires, Phys. Rev. B. 70 (24) (2004) 241303.

[49] V. Barone, O. Hod, G.E. Scuseria, Electronic structure and stability of semiconducting graphene nanoribbons, Nano Lett. 6 (12) (2006) 2748–2754.

[50] U. Khalilov, E.C. Neyts, Mechanisms of selective nanocarbon synthesis inside carbon nanotubes, Carbon. 171 (2021) 72–78.

[51] Ö. Birer, E. Yurtsever, Dimer formation of perylene: an ultracold spectroscopic and computational study, J. Mol. Struct. 1097 (2015) 29–36.

[52] D. Casanova, Theoretical investigations of the perylene electronic structure: monomer, dimers, and excimers, Int. J. Quantum Chem. 115 (7) (2015) 442–452.

[53] Y. Lai, et al., Synthesis of ultrathin nanosheets of perylene, Cryst. Growth Des. 15 (3) (2015) 1011– 1016.

[54] T. Yago, et al., Growth of β-perylene crystal, Chem. Lett. 36 (3) (2007) 370–371.

[55] D. Zahn, Thermodynamics and kinetics of prenucleation clusters, classical and non-classical nucleation, Chem. Phys. Chem. 16 (10) (2015) 2069–2075.